

## 镍基高温金属熔敷 CrFeNb 陶瓷熔合层微观组织

艾昌辉<sup>1</sup>, 赵志龙<sup>1</sup>, 苏 建<sup>1</sup>, 李景伟<sup>2</sup>

(1. 西北工业大学 机电学院, 西安 710072; 2. 西北工业大学 工程训练中心, 西安 710100)

摘 要: 采用氩弧熔焊的方法在镍基高温合金 K4169 表面熔敷高温金属间化合物 CrFeNb. 利用电镜扫描( SEM) 和能谱分析( EDS) 观察熔敷区的微观组织及元素分布. 结果表明, 基材 K4169 与高温金属间化合物 CrFeNb 之间形成了厚度约 64.8  $\mu\text{m}$  的熔合层; 熔合层中无气孔、裂纹等缺陷, 凝固的 CrFeNb 相呈枝晶状伸入基材 K4169 中并与之交错连接, 形成了良好的冶金结合; 依据原子数比例关系, 熔合层中形成了两种新的 Cr-Fe-Ni-Nb 系复合相, 分别为  $\text{Cr}_{(7.16 \sim 25.0)}\text{-Fe}_{(6.39 \sim 23.4)}\text{-Ni}_{(10.6 \sim 56.9)}\text{-Nb}$  和  $\text{Cr}_{(1.60 \sim 3.48)}\text{-Fe}_{(1.44 \sim 3.11)}\text{-Ni}_{(2.84 \sim 7.20)}\text{-Nb}$ .

关键词: 氩弧熔焊; 金属间化合物; 熔合层; 凝固

中图分类号: TG174.4 文献标识码: A 文章编号: 0253-360X(2011)09-0061-04



艾昌辉

## 0 序 言

高温合金由于具有较高的高温强度、良好的疲劳性能和断裂韧性等特点而得到广泛应用,但在高温或在温度交替变化的条件下工作,因工作过程中反复急剧的冷热变化形成相当大的热应力而易造成疲劳破坏,从而限制了其在高温下的使用. 而金属间化合物原子的长程有序排列和原子间金属键与共价键共存的特性,使其性能介于金属和陶瓷之间,被誉为半陶瓷材料,具有良好的高温抗氧化性及耐磨性. 因此在金属表面加涂金属间化合物陶瓷涂层,制备既具有金属的强度和韧度又具有陶瓷材料耐高温、高温抗氧化、耐磨、耐腐蚀等优点的一种新型复合材料,正越来越受到人们的重视<sup>[1-3]</sup>. 熔敷陶瓷的金属材料可应用于工模具及特殊工况的结构件,如飞机涡轮发动机叶片、电厂汽轮机叶片和鼓风机叶片等<sup>[4-6]</sup>. 然而熔敷涂层的性能很大程度上受到两者结合状态的影响,研究熔敷界面结合区域的微观组织结构和元素扩散情况是判断两种材料结合状态的重要依据.

钨极氩弧焊具有短时间高能量密度,对熔化金属存在剧烈的搅拌作用,因此采用氩弧熔焊工艺可将高温合金和金属间化合物同时熔化,并利用其对

熔化金属的搅拌作用获得良好的熔焊组织. 以镍基高温合金 K4169 为基材和高温金属间化合物 CrFeNb 为涂覆材料,采用氩弧熔焊工艺,对 K4169 和 CrFeNb 两材料间的熔焊润湿性开展研究,并通过对熔焊层微观组织形貌和成分进行分析,研究了熔合层的微观组织形貌及其相组织分布特征.

## 1 试验方法

将镍基高温合金 K4169 基材制成  $\phi 30 \text{ mm} \times 10 \text{ mm}$  的圆柱体铸锭,敷材 CrFeNb 为块状固体. 两者的化学成分如表 1 所示.

表 1 试验材料的化学成分(质量分数, %)

Table 1 Chemical composition of materials

	Cr	Fe	Nb	Ni	Mo	余量
K4169	18.4	19.6	5.3	52	3.1	1.6
CrFeNb	29	28	43	—	—	—

对基材表面进行清整、粗化处理. 采用预置法,用水玻璃将敷材粘结在基材表面,烘干. 熔敷试验采用 YC-300WX4 型钨极氩弧焊机,高纯氩气作为保护气体,氩弧电流 100 A,氩气流量 10 L/min,使高温金属间化合物 CrFeNb 充分熔敷在基材表面.

采用电火花线切割沿垂直于熔合层方向剖分加工出横截面试样,经研磨、抛光后,用稀释 10 倍的王水进行化学腐蚀. 采用 JXA-840 型扫描电镜( SEM)

收稿日期: 2010-07-12

基金项目: 国家重点基础研究发展计划( 2006CB605202-2); 国家自然科学基金资助项目( 50874093); 高档数控机床与基础制造装备科技重大专项( 2009ZX04006-042)

观察熔合层的组织和形貌,用 SEM 附带的能谱分析仪(EDS)分析熔合层组织的成分及元素扩散情况。

## 2 试验结果与讨论

### 2.1 熔合层组织与元素扩散分析

图 1 是 K4169 基材表面熔敷高温金属间化合物 CrFeNb 合金所得熔合层的横截面形貌。由图 1 可明显看出,熔焊组织可分为三层结构,上部细小胞状晶组织为敷材 CrFeNb,下部黑色组织为基材 K4169,中间是厚度约  $64.8\ \mu\text{m}$  的熔合层,且熔合层组织致密均匀,无气孔、裂纹等缺陷。界面层处,凝固的 CrFeNb 相呈枝晶状伸入基材 K4169 内部,并与之交错分布,说明敷材 CrFeNb 对基材 K4169 的渗透性和浸润性较好。熔合层上部靠近敷材 CrFeNb 处存在大量细小的胞状晶组织,最小晶粒度可达  $3\ \mu\text{m}$ 。这主要是因为氩弧熔敷结束后,熔池表面迅速凝固,形成封闭熔池。熔池中的热量主要由基材和空气传导,而镍基高温合金 K4169 高温导热率较低,阻碍了热量的快速传递,减小了温度梯度,故界面处不具备形成平面晶的条件,而形成细小胞状晶组织。

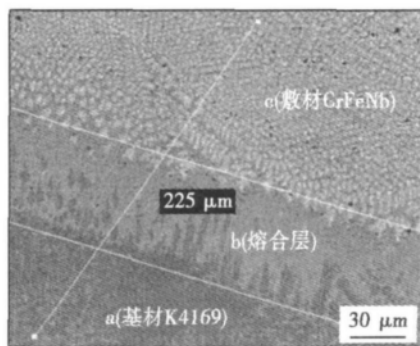


图 1 熔合层横截面的组织形貌及扫描位置

Fig. 1 Cross-section micrograph of cladding coating

图 2 为沿图 1 中所示的线扫描轨迹作 SEM 线扫描(a→b→c 与图 1 分层标号对应)测得的 Cr、Fe、Ni 和 Nb 元素分布曲线。由 Cr、Fe 元素线扫描图(图 2a)可以看出,熔敷后,熔合层 b 两侧的基材 K4169 与敷材 CrFeNb 中的 Cr、Fe 元素含量大致相等,而敷材 CrFeNb 中 Cr 和 Fe 元素的含量略高于基材(表 1),表明 Cr 和 Fe 元素发生了扩散。图 2b 显示 Nb 元素在基材一侧的含量较低,且其过渡曲线发生陡变,说明 Nb 元素在从敷材至基材的扩散过程受阻,仅发生少量扩散。这主要是因为基材 K4169 在熔敷过程中处于微熔或不熔,结构相对较为致密,且 Nb 原子

半径较大,造成 Nb 原子向基材时的扩散受阻。Ni 元素在基材一侧的含量很高,并且 Ni 元素的过渡曲线并非是一条陡变的垂直线,而是约有  $65\ \mu\text{m}$  的元素过渡区,说明在熔合层与基材的界面结合处存在一个区域很窄的共混区,发生了原子扩散。

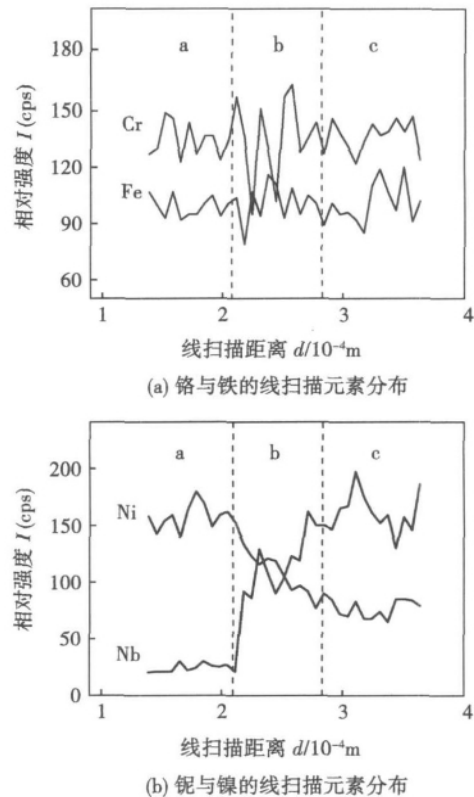


图 2 电子显微镜(SEM)线扫描元素分布

Fig. 2 Line-scan(SEM) distribution of Cr, Fe, Nb, Ni

熔敷时,钨极氩弧焊的热量迅速加热敷材至熔化状态,由于基材熔点略低于敷材,基材上表面也必然局部熔化,并与熔化的敷材在基材上表面形成熔池。熔池内液态金属在电弧的机械力、气流的吹力、电磁力等,以及在不均匀温度分布导致的金属密度差和表面张力差的作用下,处于不断的搅拌和对流运动状态。在熔池液态金属的冲刷作用下,熔池底部附近形成小岛、半岛、后续熔化滞留层等形貌<sup>[7]</sup>。凝固时,不均匀混合区的熔池底部液态金属以不完全熔化区未熔化的基材金属晶粒边界为凝固形核的现成表面,以联生方式生长,形成熔合区。凝固的 CrFeNb 相包围熔池底部的小岛、半岛和后续熔化滞留层,从而形成冶金嵌套结构。

熔合层将基材与敷材分离,而两侧合金元素浓度梯度较大,熔焊过程中,熔池内金属在多种力的作用下处于对流运动状态,其结果是短时间内促使合金元素(主要为 Cr、Fe、Ni、Nb 元素)发生扩散,在基

材与敷材两相之间形成元素扩散层,并伴随有各种物理、化学反应。

结合图 1 和图 2 可知,表层熔焊层和基材 K4169 之间相互熔合,具有较强的结合力,属于冶金结合<sup>[8]</sup>。

2.2 熔合层相组成分析

图 3 为基材 K4169 表面熔敷 CrFeNb 合金所得熔合层的高倍率 SEM 形貌及能谱分析。图 3b,图 3c,图 3d,图 3e 分别为图 3a 中点 3、6、8、9 区域

对应的元素能谱分析,其中点 3、6 区域对应图中所示黑色组织,点 8 区域对应白色组织,点 9 区域对应胞状晶组织。可以看出,该四处区域均主要由 Cr、Fe、Nb 和 Ni 四种元素组成,但各元素含量明显不同。点 3、6 区域中 Nb 元素含量明显低于点 8、9 区域,而 Ni 元素含量却偏高。这表明图 3 中所示的黑色组织和白色组织均为 Cr-Fe-Nb-Ni 系合金,之所以颜色不同是因为所对应区域处形成新相的各元素含量不同。

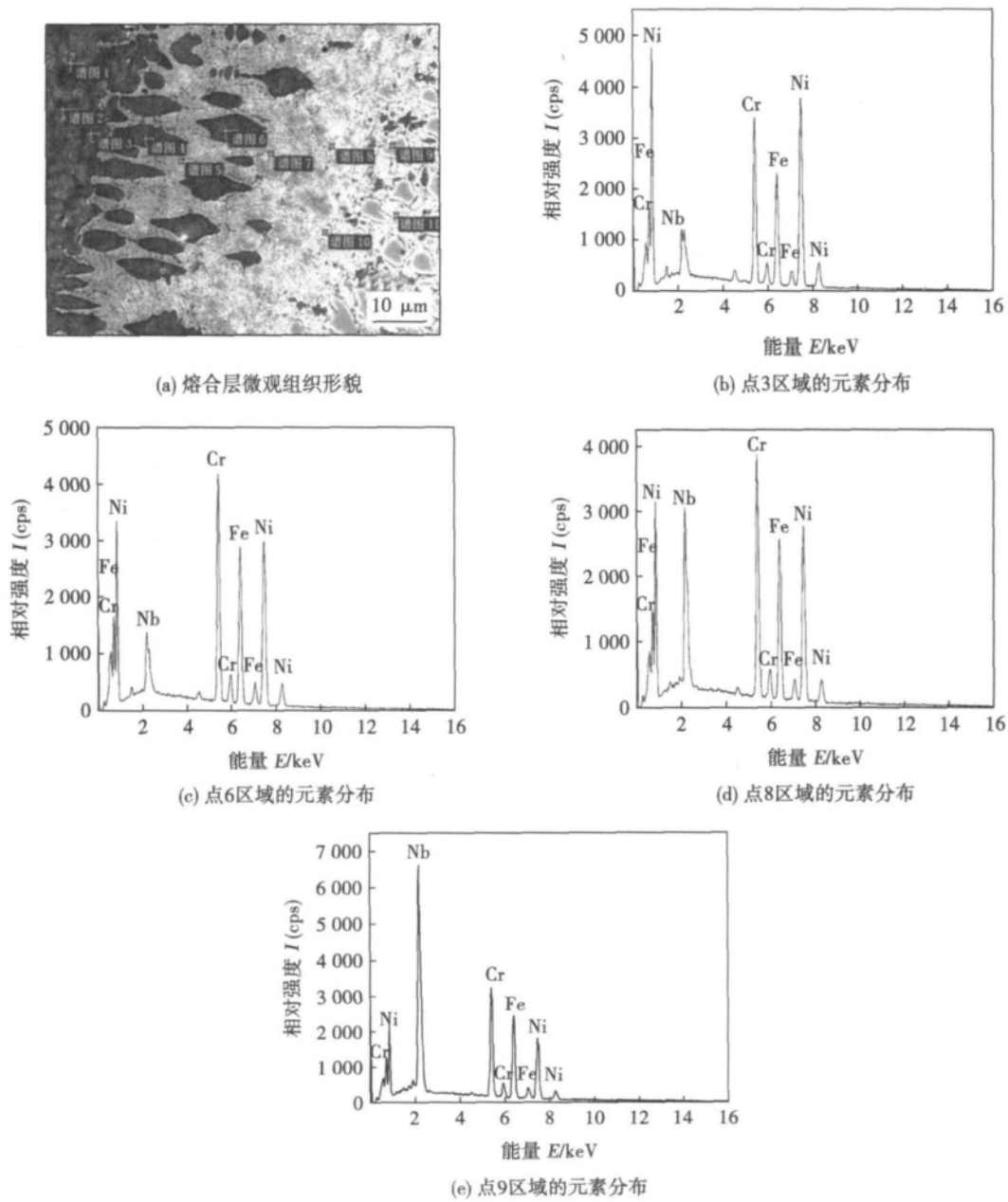


图 3 熔合层微观组织形貌和能谱分析

Fig. 3 Microstructure and element analysis of fusion layer

表 2 为图 3a 中所对应区域的面扫描元素含量。根据表 2 可计算得出各区域处所对应的原子个数

比,黑色组织为  $\text{Cr}_{(7.16 \sim 25.0)}\text{-Fe}_{(6.39 \sim 23.4)}\text{-Ni}_{(10.6 \sim 56.9)}\text{-Nb}$ ,白色组织为  $\text{Cr}_{(1.60 \sim 3.48)}\text{-Fe}_{(1.44 \sim 3.11)}\text{-Ni}_{(2.84 \sim 7.20)}\text{-}$

Nb 细小胞状晶组织 Cr、Fe、Ni 和 Nb 原子个数比例约为 1:1:1:1,为 Cr-Fe-Ni-Nb。其中,点 4 和 6 区域、点 8 和 11 区域处所对应的能谱分析表明,各元素含量基本相等,表明在点 4 和点 6 区域间的黑色组织以及在点 8 和点 11 区域间白色组织均形成了较稳定的化合物,分别为  $\text{Cr}_{7.31}\text{-Fe}_{6.77}\text{-Ni}_{10.66}\text{-Nb}$  和  $\text{Cr}_{2.41}\text{-Fe}_{2.16}\text{-Ni}_{3.33}\text{-Nb}$ 。这表明 Cr、Fe、Ni 和 Nb 元素的相互作用形成了复杂的固溶体,这些固溶体相互混合形成新相,其原因是熔池凝固时间短,因而体系中各组元间的元素来不及充分扩散,造成了熔合层的化学不均匀性。由此也可认为 K4169 和 CrFeNb 是由  $(\text{Cr})_x(\text{Fe})_y(\text{Ni})_m(\text{Nb})_n$  的复合相连接的。两相之间既有机械结合,又有化学结合,存在有化学键,因而两者结合牢固。

表 2 面扫描元素含量(质量分数,%)  
Table 2 Aera-scan results of fusion layer

	Cr	Fe	Ni	Nb	总含量
谱图 1	20.77	19.96	48.58	10.69	100.00
谱图 2	21.49	21.63	55.34	1.54	100.00
谱图 3	21.10	19.76	54.00	5.14	100.00
谱图 4	25.43	24.73	43.50	6.34	100.00
谱图 5	19.68	19.03	39.40	21.89	100.00
谱图 6	25.74	25.60	42.37	6.29	100.00
谱图 7	22.20	21.47	37.30	19.03	100.00
谱图 8	23.44	22.63	36.56	17.37	100.00
谱图 9	19.45	21.37	22.51	36.67	100.00
谱图 10	19.27	20.93	23.21	36.59	100.00
谱图 11	22.51	23.30	35.94	18.25	100.00

3 结 论

(1) 以高温金属间化合物 CrFeNb 为敷材,采用氩弧熔敷工艺在基材 K4169 表面制备出厚度约 64.8 μm 的熔合层。界面层处,凝固的 CrFeNb 相呈枝晶状伸入基材 K4169 内部并与之交错分布,熔合层中无气孔、裂纹等缺陷存在,形成了紧密牢固的冶金结合。

(2) 熔合层中形成了两种新的 Cr-Fe-Ni-Nb 系复合相,分别为  $\text{Cr}_{(7.16\sim25.0)}\text{-Fe}_{(6.39\sim23.4)}\text{-Ni}_{(10.6\sim56.9)}\text{-Nb}$  和  $\text{Cr}_{(1.60\sim3.48)}\text{-Fe}_{(1.44\sim3.11)}\text{-Ni}_{(2.84\sim7.20)}\text{-Nb}$ 。

参考文献:

[1] 荣鼎慧,刘英才,周拥军,等. 感应重熔 Fe-Al 金属间化合物涂层的制备及性能研究[J]. 兵器材料科学与工程,2009,32(2): 84-86.  
Rong Dinghui, Liu Yingcai, Zhou Yongjun, et al. Preparation and performance of Fe-Al intermetallic compound coating by induction remelting[J]. Ordnance Material Science and Engineering, 2009, 32(2): 84-86.

[2] Kohnle C, Mintchev O, Brunner D, et al. Fracture of metal/ceramic interfaces[J]. Computational Materials Science, 2000, 19: 261-266.

[3] Zhang Yong, Feng Di, He Zhiyong, et al. Progress in joining ceramics to metals[J]. Journal of Iron and Steel Research International, 2006, 13(2): 1-5.

[4] 李志君,吴玉萍. 等离子熔覆超厚金属-陶瓷梯度涂层的工艺与组织[J]. 机械工程材料,2007,31(11): 52-54.  
Li Zhijun, Wu Yuping. Gradient microstructure and processing of TiC-reinforced Ni-alloy extraordinary thick composite coating[J]. Materials for Mechanical Engineering, 2007, 31(11): 52-54.

[5] 朱警雷,黄继华,王海涛,等. 反应等离子喷涂 TiC/Fe-Ni 金属陶瓷复合涂层的显微组织[J]. 中国有色金属学报,2008,18(1): 36-41.  
Zhu Jinglei, Huang Jihua, Wang Haitao, et al. Microstructures of TiC/Fe-Ni metal ceramic composite coatings by reactive plasma spray[J]. The Chinese Journal of Nonferrous Metals, 2008, 18(1): 36-41.

[6] Serdar Salman, Ramazan Köse, Levent Urtekin, et al. An investigation of different ceramic coating thermal properties[J]. Materials and Design, 2006, 27: 585-590.

[7] 张汉谦. 钢熔焊接头金属学[M]. 北京: 机械工业出版社, 2001.

[8] 王立梅. 反应等离子熔敷原位合成高铬铁基复合涂层高温抗氧化性[J]. 焊接学报,2009,30(1): 93-95.  
Wang Limei. Oxidation resistance of reactive plasma cladding high-chromium iron-base composite coating[J]. Transactions of the China Welding Institution, 2009, 30(1): 93-95.

作者简介: 艾昌辉,男,1985 年出生,硕士研究生. 研究方向为智能制造与制造检测,承担 1 项国家自然科学基金资助项目的研究. 发表论文 1 篇. Email: achuizzia1985@sina.com

通讯作者: 赵志龙,男,教授,硕士生导师. Email: zhaolong@nwpu.edu.cn

arc length control; pulsed MIG welding

#### Effect of current field on Ti/TiAl interface and mechanical performance

LIU Zefeng, CHEN Shaoping, LIANG Lian-jie, MENG Qingsen ( Department of Material Science and Engineering, Taiyuan University of Technology, Taiyuan 030024, China). p 57 – 60

**Abstract:** Ti /TiAl gradient materials were prepared by field-activated pressure-assisted synthesis ( FAPAS) process. The microstructure, phase composition and fracture morphology of the interface were analyzed by SEM and XRD. The bending strength of the sample was tested by three-point bending test. Meanwhile, finite element analysis with ANSYS code was used to calculate the mechanical properties such as residual stress and deformation. It was shown that fine TiAl particles were formed with FAPAS and maximum bending strength as high as 346 MPa was obtained in the Ti/TiAl interface. The interface were layered gradient structure of TiAl/Ti<sub>3</sub>Al/Ti ( ss. Al) /Ti. The fracture located in the TiAl-Ti<sub>3</sub>Al interface, and showed brittle fracture morphology. The maximum residual stress sited in the TiAl-Ti<sub>3</sub>Al interface, which was the position of weakness of the material.

**Key words:** field-activated; finite element analysis; diffusion bonding; residual stress

#### Microstructure analysis of fusion layer melted CrFeNb on Ni-base superalloy

AI Changhui<sup>1</sup>, ZHAO Zhilong<sup>1</sup>, SU Jian<sup>1</sup>, LI Jingwei<sup>2</sup> ( 1. School of Mechatronics, Northwestern Polytechnical University, Xi'an 710072, China; 2. Engineering Training Center, Northwestern Polytechnical University, Xi'an 710100, China). p 61 – 64

**Abstract:** A coating has been made on K4169 substrate by argon arc cladding technique with the inter-metallic compound ( IMC) of CrFeNb. The microstructure and element distribution of the cladding coating were analyzed by scanning electron microscope ( SEM) and energy-dispersive spectrum ( EDS). The results showed that a fusion layer with a thickness of 64.8 μm was formed between the K4169 substrate and CrFeNb. In the fusion layer, the dendritic solidification of cladding CrFeNb stretched into the substrate and cross joined, which formed favorable metallurgical conjunction without the metallurgical defects such as alveolate air holes or cracks. According to the proportion relationship of atomic numbers, two new composite phases of Cr-Fe-Ni-Nb were formed in the fusion layer, and the calculated results showed that they were Cr<sub>(7.16~25.0)</sub>-Fe<sub>(6.39~23.4)</sub>-Ni<sub>(10.6~56.9)</sub>-Nb and Cr<sub>(1.60~3.48)</sub>-Fe<sub>(1.44~3.11)</sub>-Ni<sub>(2.84~7.20)</sub>-Nb, respectively.

**Key words:** argon arc; inter-metallic compounds; fusion layer; solidification

#### Microstructure and mechanical properties of ZrO<sub>2</sub> ceramic and kovar brazed joints

LIN Xiaochao, CAO Jian, ZHANG Lixia, Feng Jicai ( Key Laboratory for Advanced Welding Production Technology, Harbin Institute of Technology, Harbin 150001, China). p 65 – 68

**Abstract:** Brazing of ZrO<sub>2</sub> ceramic to Kovar alloy was successfully realized by using self-developed Ag-Cu-TiH<sub>2</sub> filler powder at the 825 ~ 960 °C for 1 ~ 60 min. Interface microstructures were investigated by scanning electron microscopy, X-ray diffraction and EDS energy spectrum. The results showed that the typical interface microstructure of brazed joints from Kovar side

to ZrO<sub>2</sub> ceramic side could be expressed as Kovar/Ag( s. s) + Cu( s. s) + TiFe<sub>2</sub>/TiNi<sub>3</sub> + TiFe<sub>2</sub> + Ti-Fe-Ni/Ag( s. s) + Cu( s. s) + TiFe<sub>2</sub>/Cu<sub>2</sub>Ti<sub>4</sub>O/TiO + Zr<sub>3</sub>O<sub>5</sub>/ZrO<sub>2</sub>. The maximum shear strength of the joints was 134 MPa, which was achieved when the brazing temperature was 875 °C and holding time was 10 min. The brittle fracture took place on the TiC interface. When the brazing temperature and holding time changed, the brazed joints weakened and the shear strength decreased.

**Key words:** ZrO<sub>2</sub> ceramic; Kovar alloy; brazing; interfacial microstructure; shear strength

#### Effect of micro B on wettability of Cu-P based quenching filler metals

ZOU Jiasheng, XU Xiangping, WANG Lei ( Provincial Key Lab of Advanced Welding Technology, Jiangsu University of Science and Technology, Zhenjiang 212003, China). p 69 – 72

**Abstract:** Three different components of the Cu-P based filler metal foils were prepared by single-roll rapidly-cooled equipment. The melting feature and structure were analyzed with DTA and XRD methods. The wettability of Cu-P based filler metals on copper was studied. The results showed that, compared with the conventional filler metals, the quenching filler metals had lower melting temperature and narrower melting temperature range. The quenching filler metal containing 0.03% B had the lowest liquidus temperature and the narrowest melting temperature range. The structures of the quenching filler metals with 0.03wt% B and 0.04% B were amorphous. In the same process conditions, the quenching filler metal contained 0.03wt% B had best wettability on copper. As with brazing temperature and time increased, the wettability of Cu-P based quenching filler metal appears increased first and then decreased. Compared with conventional brazing filler metals, the wettability of quenching filler metal has been improved significantly.

**Key words:** Cu-P based filler metal; quenching; amorphous filler metal; wettability

#### Microstructure of Ti/Al dissimilar alloys lap joint made by friction stir welding

CHEN Yuhua, NI Quan, HUANG Chunping, KE Liming ( National Defense Key Disciplines Laboratory of Light Alloy Processing Science and Technology, Nanchang Hangkong University, Nanchang 330063, China). p 73 – 76

**Abstract:** Dissimilar metals of TC1/LF6 were lap jointed by friction stir welding ( FSW) and the microstructure of the lap joint was studied. The results showed that good appearance of weld joint without defects such as cavitation and crack was obtained when the rotation speed of stir head was 1 500 r/min and the welding speed was 60 mm/min. Ti alloy and Al alloy intensively mix and form nugget zone in the lap zone. Ti alloy which is stirred into Al alloy on both sides of the nugget bends under the extrusion effect of the pin and tight couples with Al alloy. The microstructure in the interfacial zone of the lap joint center is lamellar structure and can be divided into three layers. The layer closed to the nugget zone and TC1 base metal is black and white stripped structure which contains Ti-Al intermetallic compound generated during FSW. The layers in the center are black lamellar structure and stripped structure with black particles distributing on the gray matrix. Black lamellar structure is TC1 base metal which is stirred into the interfacial zone, and the stripped structure with black particles distributing on the gray matrix is